



# PROPOSAL OF PROCEDURE FOR IDENTIFICATION OF MENÉTREY–WILLAM (M-W-3) PLASTICITY SURFACE OF HOMOGENEOUS AND HOLLOW MASONRY UNITS

Radosław JASIŃSKI\*

*Department of Building Structures, Silesian University of Technology, ul. Akademicka 5, 44-100 Gliwice, Poland*

Received 14 October 2018; accepted 18 January 2019

**Abstract.** The article presents the author's proposal to determine the parameters of the Menétrey–Willam (M-W-3) plasticity surface of the homogeneous masonry elements made of autoclaved aerated concrete (AAC) and vertically hollow calcium-silicate (Ca-Si) masonry units. The uniaxial and triaxial tests of AAC samples in a standard Hoek's cell was performed while the hollow units made of silicate were tested on a custom-made test stand. By performing statistical analyses, the shape of the meridians of the surface was determined, and then the eccentricity  $e$  of the elliptical function was identified.

**Keywords:** Menétrey–Willam plasticity surface, uniaxial test, triaxial test, AAC masonry unit, hollow silicate masonry units.

## Introduction

Numerous methodologies can be used in numerical analyses of masonry structures. In the engineering applications that allow current design standards linear elastic material models are used (Kubica, 2003). On the other hand, when it comes to the analysis of morphology of cracking and the failure mechanism that form the basis of scientific studies, the choice of use falls on the advanced material models implemented in micro, macro or meso masonry models taking into account the fragile properties of masonry based on the Coulomb's ideas (Majewski, 2003; Małyszko, Jemiolo, Bilko, & Gajewski, 2015). The Drucker-Prager, Hofman, Willam-Warnke, Barcelona (Drobiec, 2013; Małyszko et al., 2015; Wawrzynek & Cińcio, 2005) and the Menétrey–Willam (M-W-3) models are used, among others. With the exception of some independent solutions (Majewski, 2003; Jasiński, Drobiec, & Piekarczyk (2016a) only the M-W-3 model allows one to adjust the surface shape to the test results of masonry elements and mortar. No major technical problems arise while determining the parameters of the M-W-3 surface of homogeneous masonry units, such as brick or concrete. The classic Hoek or Karmann pressure cells can be used allowing for bi- or triaxial testing of material samples. In the case of vertically hollow masonry units (Jasiński et al., 2016a, 2016b) marked by evident orthotropy the use of the standard

pressure cells is not possible. It is necessary to use indirect methods consisting in matching the surface (determined on homogeneous samples taken from the masonry units) for testing of cut masonry elements (Drobiec & Jasiński, 2017). However, the most reliable method is to determine the failure surface based on the study of entire units. This paper presents the methodology for testing triaxial samples from autoclaved aerated concrete (AAC) and testing of whole calcium-silicate masonry units in a specially customized proprietary test stand (Jasiński, 2017a, 2017b). The results of the research were used in the elastic-plastic model of material (Červenka & Papanikolaou, 2008; Červenka, Pukl, Ozbolt, & Eligehausen, 1995; Červenka, 1985) implemented to FEM in the ATENA system, calibrated for shear walls (Jasiński, 2017b) and lintels cooperating with the wall (Drobiec, Jasiński, & Mazur, 2017).

## 1. The Menétrey–Willam surface

The surface of Menétrey–Willam (Menétrey & Willam, 1995) (M-W-3) is a modified version of the empirical model by Hoek and Brown (1980) (developed for rock description) amended by Weihe (1989) who introduced the elliptical function of eccentricity  $e$  depending on Lode angle  $\Theta$ . The equations of the three-parameter surface

\*Corresponding author. E-mail: [radoslaw.jasinski@polsl.pl](mailto:radoslaw.jasinski@polsl.pl)

M-W-3 is as follows:

$$f^p(\xi, \rho, \Theta) = \left( \sqrt{1.5} \frac{\rho}{k(\kappa) f_c} \right)^2 + m \left( \frac{\rho}{\sqrt{6} k(\kappa) f_c} r(\Theta, e) + \frac{\xi}{\sqrt{3} k(\kappa) f_c} \right) - c(\kappa) = 0, \quad (1)$$

where:

$$m = 3 \frac{(k(\kappa) f_c)^2 - (\lambda_t f_t)^2}{k(\kappa) f_c \lambda_t f_t} \frac{e}{e+1} - \text{a parameter equivalent to cohesion}; \quad (2)$$

$$r(\Theta, e) = \frac{4(1-e^2)\cos^2\Theta + (2e-1)^2}{2(1-e^2)\cos\Theta + (2e-1)\sqrt{4(1-e^2)\cos^2\Theta + 5e^2 - 4e}} - \text{elliptical function} - \text{Figure 2}; \quad (3)$$

$e$  – eccentricity of the elliptical function assuming values from the range  $e \in (0,5; 1,0)$ ;

$f_c, f_t$  – uniaxial compressive and tensile strength;

$\lambda_t \geq 1$  – scaling parameter for M-W-3 surface.

The boundary surface M-W-3 in deviatory cross-section is composed of three tangential curves along the compressive meridians – Figure 1 whose shape is affected by the assumed eccentricity  $e$  of the elliptical function – Figure 2. When eccentricity  $e$  is equal to 0.5, the deviatory cross-section of failure surface is in the shape of an equilateral triangle, meanwhile, for  $e = 1.0$ , curves forming the deviator cross section take on a shape of circle. A curve, whose shape is similar to ellipse in the zone of biaxial compression values  $\sigma_1 - \sigma_2, \sigma_3 = 0$ , is a track of boundary surface in the plane of principal stresses. In the axial cross section, the surface is formed by parabolic meridians intersecting at the tension point corresponding to triaxial tension. The ellipse extreme corresponds to material strength to biaxial compression  $f_{bc}$ . Concrete strength to biaxial stress was empirically determined as  $f_{bc} = 1.14f_c$ , and the corresponding eccentricity of elliptical function was  $e = 0.52$ . For masonry units the majority of tests involved solidbrick (Drobiec, 2006; Jasiński, 2011). The obtained values of solid brick strength to biaxial compression  $f_{bc}$  were within the range 1.02–1.14 $f_c$ , and the corresponding eccentricity values were  $e = 0.501$ –0.511. The

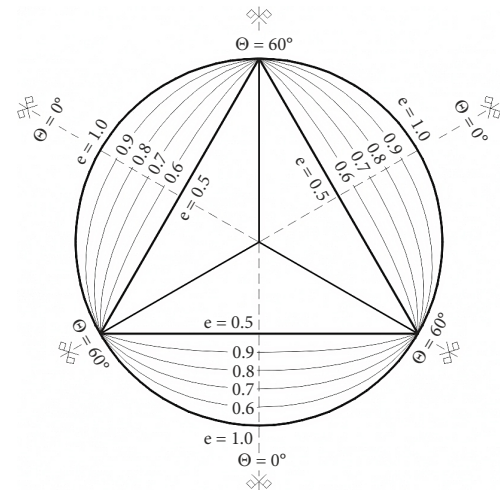


Figure 2. Shape of the elliptic function  $0,5 \geq r(\Theta, e) \geq 1,0$

Table 1. Results from strength tests on biaxial compression of solid brick and values of elliptic function

No.	Material	Author	Biaxial compressive strength $f_{bc}$	Eccentricity of elliptical function $e$
1	Solid brick	Drobiec [4]	1.02 $f_c$	0.501
2	Solid brick	Jasiński [9]	1.14 $f_c$	0.511
3	Solid brick	Szojda [18]	0.80 $f_c$	0.500

summary of the triaxial test results for solid brick is shown in Table 1. Szojda at work (Szojda, 2009) investigated two types of clay brick. Not performing biaxial studies. On the basis of the linear compression meridians, the calculated average strength for biaxial compression of both types of bricks was 0.80 $f_c$ , and the value of the eccentricity of the elliptical function was equal to  $e = 0.5$ .

The parameter of surface adjustment  $\lambda_t > 1$  determined the position of M-W-3 surfaces to the Rankine failure surface. At the value of  $\lambda_t = 1$  plasticity surface of M-W-3 was always within the Rankine pyramid, and at  $\lambda_t = 2$  surfaces intersected at the plane of hydrostatic tension and minor compression.

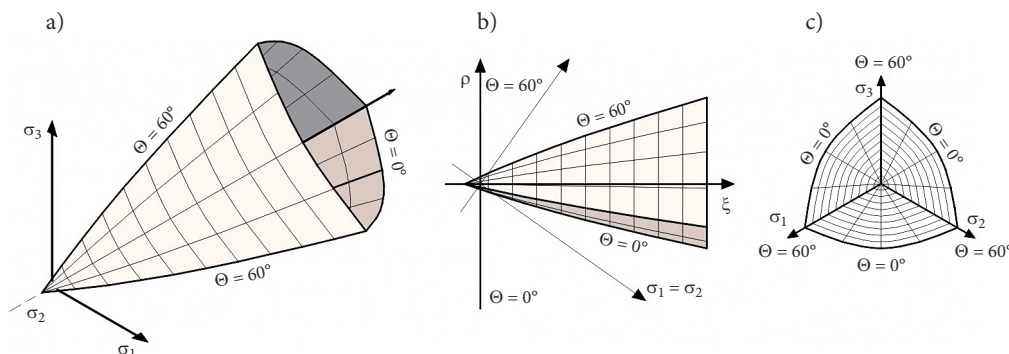


Figure 1. The Menétrey–Willam surface in the Haigh–Westergaard space: a) the view from the space of principal stresses, b) axial cross-section view, c) deviatory cross-section view

## 2. Proprietary test results

### 2.1. Tests on the autoclaved aerated concrete exposed to triaxial stress

Tests of autoclaved aerated concrete (density class 600 kg/m<sup>3</sup>, moisture 0%) were carried out in Hoek's cell on cylindrical samples 120 mm of length and Ø60 mm in diameter cut out from masonry units. The essence of the operation of Hoek's cell (Figure 3a, b) was the possibility to test the samples 1 exposed to triaxial stress where apart from the vertical load induced in the testing machine it was possible to create a simultaneous horizontal load perpendicular to the vertical axis of the sample.

The vertical loads 10 were transmitted to sample 1 from a testing machine with a range of 4000 kN by steel pistons 6, spherical bearings 5 and Teflon washers 4. Meanwhile, the horizontal side loads of the sample were developed hydraulically by introducing the fluid from the hydraulic cylinder 9 between the steel body of the device 8 and the deformable polyurethane shell of the sample 7 under pressure. Prior to the tests the surfaces of the sample bases – 1 were additionally smoothed and the four vertical grooves were made on the side walls. Then, two vertical and horizontal electro-resistant strain gauges 2 with a 20 mm base were glued to the cylinders used to measure the deformation of the mortar, and the strain gauge wires 3 were taken outside of the device through the previously made vertical grooves located on the side of the samples and the steel piston of the device.

The tests were carried out with two different stress combinations. In the first combination, the failure of the samples took place by increasing the vertical stresses and maintaining constant values of horizontal (radial) stresses. In the second combination the failure of the samples was obtained by increasing the horizontal (radial) stresses under constant vertical stresses. 12 cylindrical samples were prepared divided into two six-unit series marked as TABK – I and TABK – II. In the series marked as I the vertical stresses  $\sigma_{ver}$  were increased until failure under the constant horizontal stresses set at  $\sigma_{rad} = 0.3f_b$ ;  $0.5f_b$ ;  $0.7f_b$ . In the series II another six samples loaded with horizontal stress  $\sigma_{rad}$  were tested with constant vertical stress values of  $\sigma_{ver} = 0$ ;  $0.3f_b$ ;  $0.6f_b$ . Figure 4 presents the results of measurements of vertical and horizontal stresses of all samples of the material of the masonry units of the series I and II. In the series I compared to the strengths obtained in the uniaxial state of stress the increase in the maximum values of vertical compressive stresses was  $3.0f_b$ . Also in the remaining samples compressed vertically and horizontally at constant side stresses the increase in the value of the vertical compressive stresses was  $(1.9 - 2.6)f_b$ . Lesser increases in strength were found in the series II in which the samples underwent failure by increasing the value of horizontal stresses at constant vertical stresses. The strength of the samples in the biaxial state of stress was approximately  $1.1f_b$ . The test results are listed in Table 2.

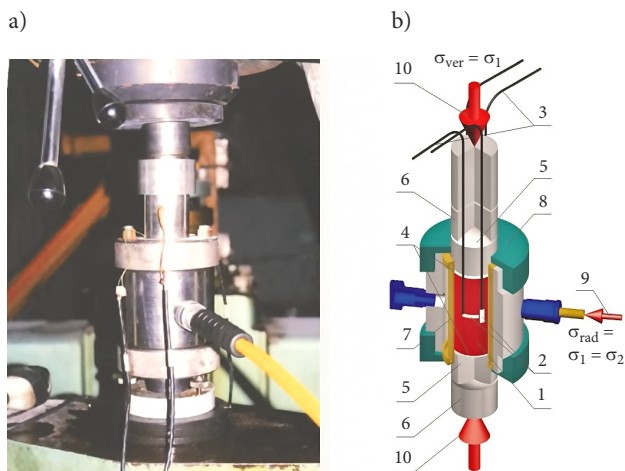


Figure 3. Hoek's cell used for triaxial compression of autoclaved aerated autoclaved concrete: a) view of the sample during the tests, b) outline (described in the text)

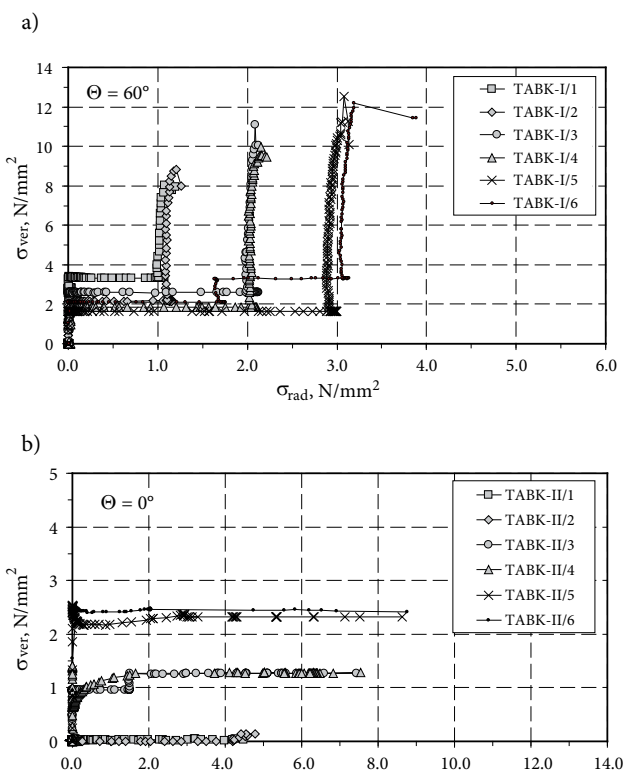
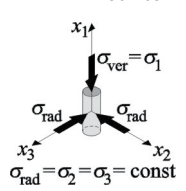
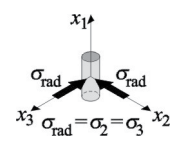


Figure 4. Relationship  $\sigma_{ver} - \sigma_{rad}$  of AAC specimens (description in the text)

### 2.2. Tests on the silicate masonry units exposed to triaxial stress

The masonry unit that had a length of 0.25 m, a height of 0.24 m and a thickness of 0.18 m with the volume of vertical holesequal to 26%, moisture 0% was used for the tests of the calcium-silicate masonry units. The experiments were performed using a test stand particularly built for that purpose, it is shown in Figure 5. The whole masonry unit 1 was placed on the heavy weight bases of the

Table 2. Results of triaxial tests of masonry units from autoclaved aerated concrete

Meridian	Series	Specimen identification	Vertical stress	Horizontal stress		Haigh-Westergaard coordinates	
			$\sigma_{ver} = \sigma_1$ N/mm <sup>2</sup>	$\sigma_{rad,I} = \sigma_2$ N/mm <sup>2</sup>	$\sigma_{rad,II} = \sigma_3$ N/mm <sup>2</sup>	$\xi$ N/mm <sup>2</sup>	$\rho$ N/mm <sup>2</sup>
Compressive meridian	TABK-I series 	TABK-I/1	8.03	1.08	1.08	5.88	5.68
		TABK-I/2	8.82	1.21	1.21	6.48	6.22
		TABK-I/3	11.11	2.09	2.09	8.83	7.37
		TABK-I/4	9.53	2.16	2.16	8.25	6.39
		TABK-I/5	12.54	3.08	3.08	10.79	7.72
		TABK-I/6	12.19	3.19	3.19	10.72	7.35
	Axial compression $f_b = f_c = 4.25$ N/mm <sup>2</sup>	1	4.87	0	0	2.81	3.98
		2	4.37	0	0	2.52	3.57
		3	3.96	0	0	2.28	3.23
		4	4.22	0	0	2.44	3.45
		5	4.03	0	0	2.33	3.29
		6	4.06	0	0	2.34	3.31
		7	4.24	0	0	2.45	3.46
Tensile meridian	TABK-II series 	TABK-I/1	0.04	4.49	0	5.20	-3.63
		TABK-I/2	0.14	4.78	0	5.60	-3.79
	Biaxial compression $f_{cb} = 4.63$ N/mm <sup>2</sup>	TABK-I/3	1.27	7.43	0	9.31	-5.03
		TABK-I/4	1.28	7.54	0	9.44	-5.11
		TABK-I/5	2.33	8.62	0	11.30	-5.14
		TABK-I/6	2.41	8.75	0	11.50	-5.18
	Axial tensioning $f_t = 0.61$ N/mm <sup>2</sup>	1	-0.58	0	0	-0.33	-0.47
		2	-0.57	0	0	-0.33	-0.47
		3	-0.57	0	0	-0.33	-0.46
		4	-0.69	0	0	-0.40	-0.57
		5	-0.75	0	0	-0.43	-0.61
		6	-0.52	0	0	-0.30	-0.43

stand 2 located between parts of the testing machine 3. The standard stress  $\sigma_1$  perpendicular to the supporting plane of the unit was induced by a hydraulic actuator 12 with the capacity of 1000 kN, and the exerted force was measured with electro-resistant dynamometer 13 with the 2000 kN capacity. Teflon slabs 11 were used to minimise friction on the top and bottom support area of the unit. A set of two retaining slabs 4 joined with steel rod tendons 5 with a diameter of 25 mm was used to induce standard stresses  $\sigma_2$  perpendicular to bed plane of the masonry unit. Steel brackets 6 were fixed to the plates 4, while a hydraulic actuator 8 with the capacity of 1000 kN or an electro-resistant dynamometer 9 with the capacity of 1000 kN was placed on one side of the brackets. The steel brackets 6 were equipped with steel pistons 7 jointed with

the dynamometer and the actuator on one side and steel sheets 12 on the other, to transmit load from the hydraulic actuators to the tested block and also to measure loading. The load transmitted to sheets 12 was applied to the tested block through Teflon slabs 11 which eliminated friction. Standard stresses  $\sigma_3$  perpendicular to the face of the masonry unit were induced in the same way as towards perpendicular direction to the bed surface, however, the steel brackets 10 equipped with an actuator 8a with the 300 kN capacity on one side and a dynamometer 9a with the capacity of 250 kN on the other side, were fixed to column 15 of the testing machine by steel clamps 14. The load was transmitted by steel pistons 7 to the sheets 12. Also friction at the face side was minimised by placing Teflon washers 11 on both sides of the masonry unit.

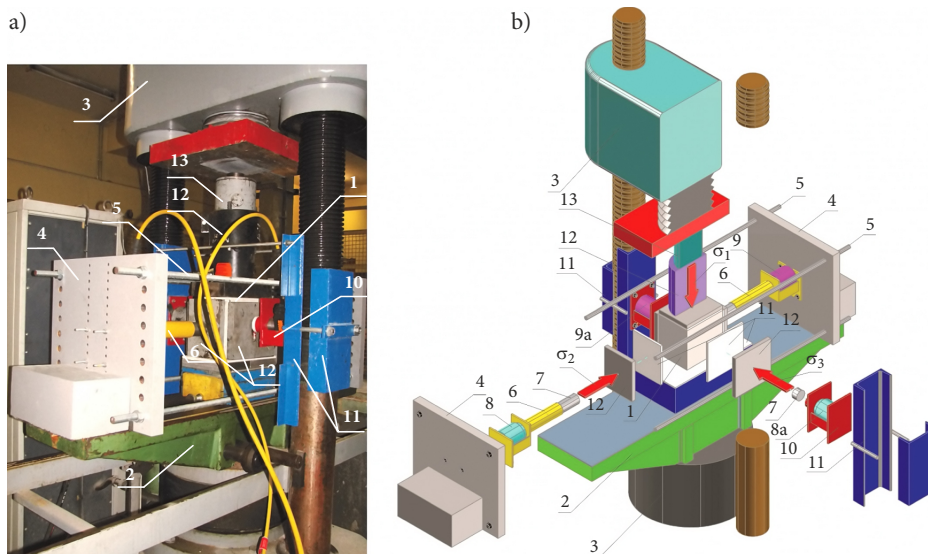


Figure 5. Test stand for masonry units exposed to triaxial stress: a) the overall view, b) the components of the test stand (described in the text)

The tests were performed on 16 masonry units grouped into 4 series symbolically identified as TSB-I, TSBIIa, TSB-IIb and TSB-III. TSB-I series included 5 masonry units, for which the vertical stress  $\sigma_{\text{ver}}$  was increased until their failure at constant horizontal stresses  $\sigma_{\text{rad,I}} = \sigma_{\text{rad,II}} = 0.007f_b$ ;  $0.009f_b$ ;  $0.08f_b$ ;  $0.12f_b$ ;  $0.18f_b$ . In order to minimise the impact of shear stresses induced by non-uniform block load at the initial phase vertical and horizontal stresses were increased uniformly until achieving the assumed value of horizontal stress  $\sigma_{\text{rad}}$ . Next, the masonry units were loaded by increasing the vertical stress  $\sigma_{\text{ver}}$  until their failure while values of the assumed horizontal stresses were achieved. The TSB-IIa series included 3 masonry units exposed to increased horizontal stress  $\sigma_{\text{rad,I}}$  until failure took place. The rest of the surfaces of those units were not loaded. Meanwhile, within the TSB-IIb series 3 masonry units underwent failure by increasing horizontal stress  $\sigma_{\text{rad,II}}$  acting on the side face of bricks. The remaining surfaces of those units were not loaded.

The TSB-III series included 5 masonry units, their failure was achieved by increasing horizontal stress  $\sigma_{\text{rad,I}}$  along the longer axis of the block (according to the arrangement in the masonry) and vertical stress to meet the condition of  $\sigma_{\text{rad,I}} = \sigma_{\text{ver}}$  during the tests. The stresses perpendicular to the side face of the unit were  $\sigma_{\text{rad,II}} = 0$ . In order to minimise the impact of shear stresses induced by uniaxial load applied to the units from the TSB-III series, horizontal and vertical stresses were applied uniformly until the unit failure took place.

Since the observation of the sample was impossible during the tests, the moment of its failure was difficult to determine on the basis of the measured loads. For this purpose, failure was regarded as a clear force drop (observed in the readings of the dynamometer). Figure 6 presents results for measured horizontal and vertical stresses for all samples from the TSB-I and TSB-III series, and the summary of the results is shown in Table 3.

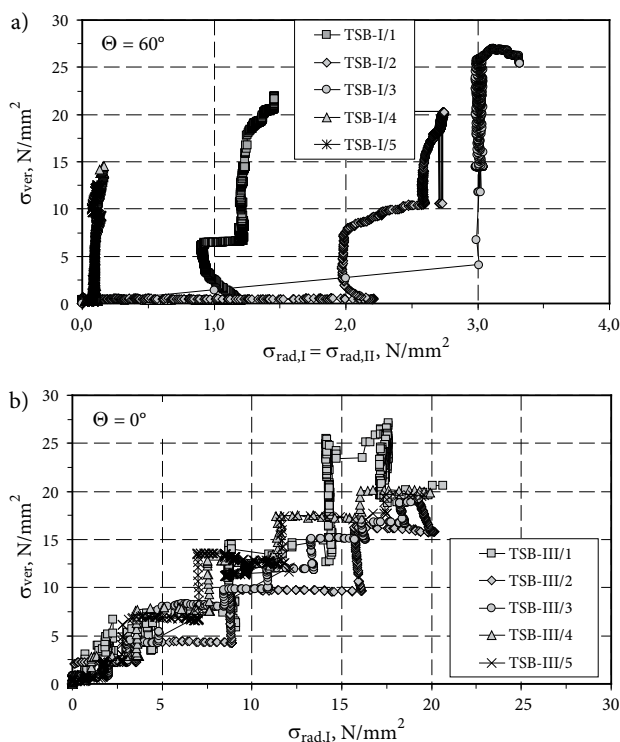
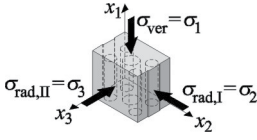
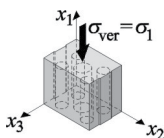
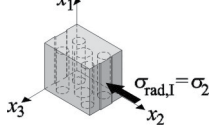
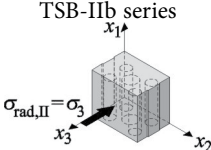
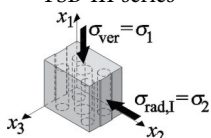
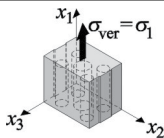
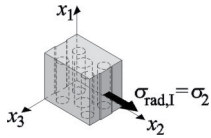
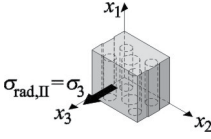


Figure 6. Relationship of  $\sigma_{\text{ver}} - \sigma_{\text{rad}}$  of the silicate masonry units of the series TSB-I and TSB-III: a)  $\sigma_{\text{rad,I}} = \sigma_{\text{rad,II}} = \text{const}$ , b)  $\sigma_{\text{ver}} = \sigma_{\text{rad,I}}$

The failure of the masonry units from TSB-I series induced by increasing vertical stress at the constant horizontal stresses was similar to that of the units in the uniaxial compression. No clear failure was observed on the support surface – Figure 7a. Another failure mechanism was found in the units of the TSB-III series to which increasing vertical and horizontal stresses were applied. At the moment of failure – Figure 7b cracks were found on each external side of the unit. The internal walls between the cavities were almost completely crushed.

Table 3. Results of the triaxial tests on calcium-silicate masonry units

Meridian	Series	Specimen identification	Vertical stress	Horizontal stress		Haigh-Westergaard coordinates		
			$\sigma_{ver} = \sigma_1$ N/mm <sup>2</sup>	$\sigma_{rad,I} = \sigma_2$ N/mm <sup>2</sup>	$\sigma_{rad,II} = \sigma_3$ N/mm <sup>2</sup>	$\xi$ N/mm <sup>2</sup>	$\rho$ N/mm <sup>2</sup>	
Compressive meridian	TSB-I series 	TSB-I/1	21.95	1.46	1.46	14.36	16.73	
		TSB-I/2	20.26	2.11	2.11	14.13	14.82	
		TSB-I/3	26.95	3.12	3.12	19.16	19.46	
		TSB-I/4	14.54	0.16	0.16	8.58	11.74	
		TSB-I/5	12.51	0.12	0.12	7.36	10.12	
	 Axial compression $f_b = f_c = 17.7$ N/mm <sup>2</sup>	1	18.23	0	0	10.53	14.88	
		2	17.78	0	0	10.27	14.52	
		3	17.38	0	0	10.03	14.19	
		4	18.02	0	0	10.40	14.71	
		5	17.76	0	0	10.25	14.50	
		6	16.93	0	0	9.77	13.82	
Compressive meridian	TSB-IIa series  $f_{c,I} = 5.04$ N/mm <sup>2</sup>	TSB-IIa/1	0	5.03	0	2.90	4.10	
		TSB-IIa/2	0	4.37	0	2.52	3.57	
		TSB-IIa/3	0	5.73	0	3.31	4.68	
	TSB-IIb series  $f_{c,I} = 7.55$ N/mm <sup>2</sup>	TSB-IIb/1	0	0	7.38	4.26	6.0	
		TSB-IIb/2	0	0	7.25	4.19	5.9	
		TSB-IIb/3	0	0	8.00	4.62	6.5	
Tensile meridian	TSB-III series  Biaxial compression $f_{cb} = 19.66$ N/mm <sup>2</sup>	TSB-III/1	20.63	20.63	0	23.82	-16.84	
		TSB-III/2	19.27	19.27	0	22.25	-15.74	
		TSB-III/3	18.88	18.88	0	21.80	-15.41	
		TSB-III/4	19.90	19.90	0	22.98	-16.25	
		TSB-III/5	19.60	19.60	0	22.63	-16.00	
	 Axial tensioning	1	$f_t \frac{f_b}{f_B} = 1.92 \frac{17.7}{24.5} = 1.39$	0	0	-0.80	-1.13	
		 Axial tensioning	2	0	$1.92 \frac{5.04}{17.7} = 0.55$	0	-0.316	-0.45
			 Axial tensioning	3	0	0	$1.92 \frac{7.55}{17.7} = 0.82$	-0.47

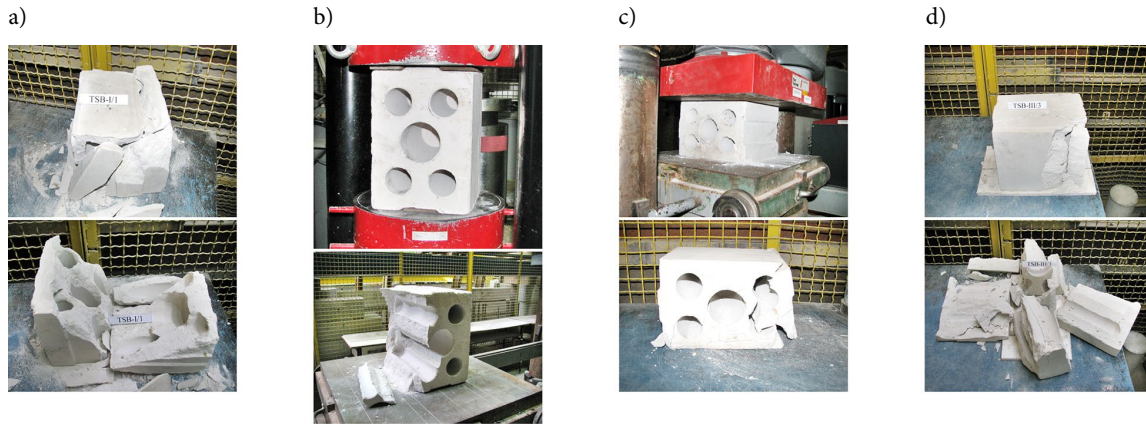


Figure 7. The view of the selected masonry units of the TSB-I, TSB-IIa and TSB-III series during and after the tests:

- a) TSB-I –  $\sigma_{\text{rad,I}} = \sigma_{\text{rad,II}} = \text{const.}$ ,  $\sigma_{\text{ver}} \neq 0$ , b) TSB-IIa –  $\sigma_{\text{rad,I}} \neq 0$ ,  $\sigma_{\text{ver}} = \sigma_{\text{rad,II}} = 0$ ,  
 c) TSB-IIb  $\sigma_{\text{rad,II}} \neq 0$ ,  $\sigma_{\text{ver}} = \sigma_{\text{rad,I}} = 0$ , d) TSB-III  $\sigma_{\text{ver}} = \sigma_{\text{rad,I}} \neq 0$ ,  $\sigma_{\text{rad,II}} = 0$ ,

### 3. Calibration of failure surface

In the presented criterion the shape of meridians forming the failure surface is not subjected to any modifications as it is determined by the uniaxial compression and tension. However, some shape corrections of M-W-3 failure surface as well as adjustments to results from testing of the material other than concrete are possible. Such corrections involve the value of eccentricity  $e$  of elliptical function, which determines the shape of failure surface at deviatory cross-section. The proper eccentricity value of the elliptical function should be selected in a way to ensure that the uniaxial tensile strength and the biaxial compressive strength are as close as possible to the tensile meridian, and the compressive strength is distributed at the compressive meridian or as close as possible to it.

An iterative procedure, based on searching for the optimum shape of compressive and tensile meridians, was used to determine the value  $e$ . Changes in the value  $e$  were made to calculate the biaxial compressive strength  $f_{\text{cb}}$  which was compared with the strength observed in the tests. Every time the average estimation error of the shape of meridians with reference to the obtained test results was calculated on the basis of results from the triaxial tests. The value  $e$ , at which the lowest percentage difference was obtained, was assumed in the further numerical calculations.

First, the Haigh-Westergaard coordinates ( $\xi$ ,  $\rho$ ,  $\Theta$ ) were used to present the obtained stress values according to the following equations:

$$\xi = \frac{I_1}{\sqrt{3}}; \quad (4)$$

$$\rho = \sqrt{2J_2}; \quad (5)$$

$$\Theta = \frac{1}{3} \arccos \left[ \frac{3\sqrt{3}J_3}{2J_2^{2/3}} \right], \quad (6)$$

where:

$I_1 = \sigma_1 + \sigma_2 + \sigma_3$  – first invariant of stress;

$J_2 = \frac{1}{6} [(\sigma_1 - \sigma_2)^2 + (\sigma_2 - \sigma_3)^2 + (\sigma_3 - \sigma_1)^2]$  – second invariant of stress;

$J_3 = (\sigma_1 - \sigma_m)(\sigma_2 - \sigma_m)(\sigma_3 - \sigma_m)$  – third invariant of stress;

$\sigma_m = \frac{1}{3} I_1$  – average hydrostatic pressure;

$\sigma_1 = \sigma_{\text{ver}}$  – vertical stress (perpendicular to the supporting plane for calcium-silicate units);

$\sigma_2 = \sigma_{\text{rad,I}}$  – horizontal stress (perpendicular to the supporting plane for silicate units);

$\sigma_3 = \sigma_{\text{rad,II}}$  – horizontal stress (perpendicular to the supporting plane for calcium-silicate units).

Load paths ( $\sigma_{\text{ver}} > \sigma_{\text{rad}}$  – TSB-I, TSB-IIa and TSB-IIb series, and  $\sigma_{\text{ver}} = \sigma_{\text{rad}}$  – series III) found in the planes inside the failure surface were used in triaxial tests on calcium-silicate units. For  $\sigma_{\text{ver}} < \sigma_{\text{rad}}$  the values of points corresponding to sample failure were at the compressive meridian for which Lode angle was  $\Theta = 60^\circ$ . Meanwhile, if  $\sigma_{\text{ver}} = \sigma_{\text{rad}}$ , then the points identifying the strength were placed at the tensile meridian, for which Lode angle was  $\Theta = 0^\circ$ . In case of the autoclaved aerated concrete, 2 series of tests were performed in the conditions where samples were tested under various combinations of vertical and horizontal stresses. For the TABK-I series vertical stresses were increased at the constant horizontal stresses ( $\sigma_{\text{ver}} > \sigma_{\text{rad}}$ ), and points distributed at the compressive meridian were identified at the failure moment. In the meantime, the sample failure in the TABK-II series was caused by increasing horizontal stresses at the constant vertical stresses ( $\sigma_{\text{ver}} < \sigma_{\text{rad}}$ ) and points at the tensile meridian were also identified. Apart from the points determined from the triaxial tests, the results of the uniaxial tests on compression and tension were also necessary for calibrating the eccentricity of elliptical function where the horizontal stress was assumed to be  $\sigma_{\text{rad}} = 0$ . Tensile strength values for calcium-silicate units were determined based on the sampled cores in axial tension. Next, tensile strength ratios along the axis of the masonry units (also

acting as orthotropic axes) were taken to be identical with those of compressive strength. Therefore, the strength values along the axis of the masonry units were calculated by multiplying the determined axial tensile strength of block material by the ratio of compressive strength towards a given direction to compressive strength of whole masonry units observed in the tests. Due to isotropy of the autoclaved aerated concrete material uniaxial compressive and tensile strengths did not require any corrections and were directly taken from the tests.

The summary of test results is presented in Tables 2 and 3, and calculations of meridian shapes are shown in Table 4. Figure 8 illustrates the calculation results and the test results as well as the trajectory of compressive and tensile meridians calculated from the following expression:

Compressive meridian:

$$\rho_c(\xi, r_c) = \frac{\sqrt{6}}{36} \left( -2r_c k(\kappa) f_c m + \sqrt{r_c^2 [k(\kappa) f_c]^2 m^2 - 12\sqrt{3} m k(\kappa) f_c \xi + 36c(\kappa) [k(\kappa) f_c]^2} \right) \quad (7)$$

Tensile meridian:

$$\rho_t(\xi, r_t) = \frac{\sqrt{6}}{36} \left( -2r_t k(\kappa) f_c m + \sqrt{r_t^2 [k(\kappa) f_c]^2 m^2 - 12\sqrt{3} m k(\kappa) f_c \xi + 36c(\kappa) [k(\kappa) f_c]^2} \right) \quad (8)$$

where:

$r_c$  – parameter of elliptical function at compressive meridian calculated from the equation (3),  $\Theta = 60^\circ$ ;

$r_t$  – parameter of elliptical function at tensile meridian calculated from the equation (4),  $\Theta = 0^\circ$ ;

$$m = 3 \frac{[k(\kappa) f_c]^2 - (\lambda_t f_t)^2}{k(\kappa) f_c \lambda_t f_t} \frac{e}{e+1} \text{ – cohesion equivalent;}$$

$k(\kappa) = 1$  – strengthening parameter at plasticisation moment;

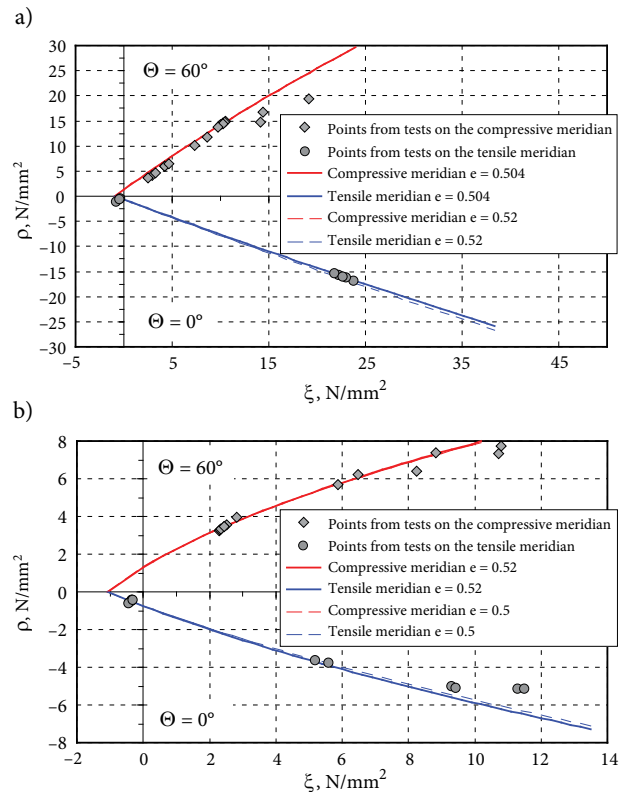


Figure 8. Uniaxial and triaxial test results as well as compressive and tensile meridians of M-W-3 surface:

- a) silicate masonry units,
- b) units made of autoclaved aerated concrete

$c(\kappa) = 1$  – weakening parameter at plasticisation time;

$\lambda_t = 1$  – scaling parameter of boundary surface;

$f_c, f_t$  – uniaxial compressive and tensile strength;

The comparison of the triaxial test results for calcium-silicate units and the autoclaved aerated concrete with calculations based on M-W-3 surface at different values of  $e$  is shown in Table 4. In addition to biaxial compression  $f_{bc,cal}$  identified from the compressive meridian, there are also values for resistance to triaxial uniform tensile strength  $f_{tt,cal}$ , which is the intersection of meridians at

Table 4. Comparison of test results in uni- and biaxial stress states of silicate masonry units and AAC masonry units with the results of calculations according to the M-W-3 surface at different values of parameter  $e$

Masonry unit	Test results			Parameter $e$	Calculation results		$\frac{f_{bc}}{f_{bc,cal}}$	average estimation error $B, \%$
	$f_{b,mv}$ N/mm <sup>2</sup>	$f_{b,pmv}$ N/mm <sup>2</sup>	$f_{bc}$ N/mm <sup>2</sup>		$f_{tt,cal}$ N/mm <sup>2</sup>	$f_{bc,cal}$ N/mm <sup>2</sup>		
calcium-silicate masonry units	17.7	0.55	19.7	0.504	0.943	19.26	1.02	14.1
				0.51	0.936	21.86	0.90	14.1
				0.52	0.92	26.72	0.74	14.2
AAC masonry units	4.25	0.62	4.63	0.50	1.09	4.25	0.92	11.6
				0.51	1.07	4.44	1.09	12.4
				0.52	1.06	4.64	1.00	13.2
				0.53	1.05	4.85	1.05	14.0



the plane of hydrostatic tension. At  $e = 0.52$  being the default eccentricity value for standard concrete, the biaxial compressive strength of silicate units calculated from the equation for tensile meridian differed from the empirical value by 36%, and the average assessment error was 14.2%. By means of reducing eccentricity to the value of  $e = 0.51$ , the similarly determined biaxial compressive strength was lower than the empirical value by only 10%, and the standard assessment error was 14.1%. The test method determined that the best strength adjustment to biaxial compression with the difference to mean value from the tests at the level of 2%, was obtained at eccentricity value  $e = 0.504$ , and standard assessment error equal to 14.1%. In the case of autoclaved aerated concrete the smallest difference in biaxial compressive strength of 0.2% and the average estimation error of 13.2% was obtained at  $e = 0.52$ , i.e. the value applied to standard concrete. With eccentricity values of  $e = 0.51$  and  $0.53$  differences between 9% and 5% were obtained and the average estimation errors were then 12.4–14%. The comparison of the obtained results of triaxial tests with the meridians of the boundary surface of the material of calcium-silicate units and the material of autoclaved aerated concrete is shown in Figure 8.

## Conclusions

Uniaxial and triaxial tests were necessary for identifying each failure surface in the Haigh-Westergaard (H-W) space. For homogeneous materials, such as concrete or rock, typical pressure cells, e.g. of Hoek or Karman type, can be used. Standard methods were not effective for masonry units, therefore, other techniques are required. Failure surface of the silicate units was identified by means of the test stand for masonry units in triaxial stress, customized and developed for the purpose of testing of such materials. The obtained test results were expressed as H-W coordinates, and the value of parameter  $e$  was chosen iteratively to the M-W-3 failure surface. The determined value was equal to  $e = 0.504$  (at the average estimation error equal to 13.2%), which approximates the shape of surface M-W-3 at deviatory cross-section to the equilateral triangle. In the case of autoclaved aerated concrete triaxial tests of samples taken from the masonry units were performed. The elliptical function value chosen iteratively  $e = 0.52$  at the average estimation error of 14.1%. In summary, the value of the elliptical function obtained in the tests of the silicate elements equal to  $e = 0.504$  led to the fact that at deviatory cross-section the surface of M-W-3 had the shape of an equilateral triangle. Meanwhile, in the case of autoclaved aerated concrete  $e = 0.52$  was obtained, which is identical to that of ordinary concrete. For solid brick the values of eccentricity of elliptical function has shown considerable variability of  $e = 0.500 - 0.511$ . In this situation unlike the ordinary concrete, in which the value of  $e$  parameter is constant, in the case of masonry units it is necessary to carry out triaxial tests to determine the appropriate shape of the M-W-3 boundary surface.

Further research in this field is necessary, both in terms of cognitive and utilitarian in order to create a broad base of results enabling numerical modeling of masonry walls. The diagnoses require not only mechanical but also statistical parameters allowing for statistical (probabilistic) analyzes. It can not be ruled out that in the case of other masonry elements, e.g. porous ceramic (or a lower production category according to EN-1996-1-1:2010), the dispersion of results will be greater, due to the complexity of the structure of the element and the quite unpredictable properties of the burnt clay. This will not change the procedure, but rather the number of test specimens and the proportion of vertical and horizontal stresses.

It is reasonable to develop empirical dependencies that take into account the shape, humidity, material density (Jasiński et al., 2019) and properties in the biaxial state. Thanks to this, FEM analyzes of existing masonry structures will be possible only on the basis of diagnostic construction tests.

## References

- Červenka, J., & Papanikolaou, V. K. (2008). Three dimensional combined fracture-plastic material model for concrete. *International Journal of Plasticity*, 24, 2192-2220. <https://doi.org/10.1016/j.ijplas.2008.01.004>
- Červenka, V., Pukl, R., Ozbolt, J., & Eligehausen, R. (1995). Mesh sensitivity effects in smeared finite element analysis of concrete structures. In *Proceedings of the 2nd International Conference on Fracture Mechanics of Concrete Structures – FraMCoS 2*, (pp. 1387-1396).
- Červenka, V. (1985). Constitutive model for cracked reinforced concrete. *Journal Proceedings*, 82(6), 877-882. <https://doi.org/10.14359/10409>
- Drobiec, Ł. (2006). FEM micro-model for masonry reinforced in bed joints. In *Proceedings of the British Masonry Society*, No. 10. The Society Stoke-on-Trent.
- Drobiec, Ł. (2013). *Przeciwdziałanie zarysowaniu ściskanych murów zbrojeniem spoin wspornych*. Gliwice: Wydawnictwo Politechniki Śląskiej (in Polish).
- Drobiec, Ł., & Jasiński, R. (2017). Adoption of the Willam-Warnke failure criterion for describing behavior of Ca-Si hollow blocks. *Procedia Engineering*, 193, 470-477. <https://doi.org/10.1016/j.proeng.2017.06.239>
- Drobiec, Ł., Jasiński, R., & Mazur, W. (2017). Precast lintels made of autoclaved aerated concrete – tests and theoretical analyses. *Cement, Wapno, Beton*, 22(5), 399-413.
- Hoek, E., & Brown, E. T. (1980). Empirical criterion for rock masses. *Journal of the Geotechnical Engineering Division*, 106(GT9), 1013-1035.
- Jasiński, R. (2011). Numerical model of the horizontally sheared wall. In *7<sup>th</sup> International Conference Analytical Models and New Concepts in Concrete and Masonry Structures AMCM 2011*, Kraków, Poland (pp. 233-234).
- Jasiński, R., Drobiec, Ł., & Piekarczyk, A. (2016a). Mechanical properties of masonry walls made of calcium silicate materials made in Poland. Part 1. Masonry properties and compressive strength. *Procedia Engineering*, 161, 904-910. <https://doi.org/10.1016/j.proeng.2016.08.755>

- Jasiński, R., Drobiec, Ł., & Piekarczyk, A. (2016b). Mechanical properties of masonry walls made of calcium silicate materials made in Poland. Part 2. Shear and flexural strength. *Procedia Engineering*, 161, 911–917. <https://doi.org/10.1016/j.proeng.2016.08.756>
- Jasiński, R. (2017a). Identification of the parameters of Menétrey–Willam failure surface of calcium silicate units. IOP Publishing. *IOP Conference Series: Materials Science and Engineering*, 245, 032045. <https://doi.org/10.1088/1757-899X/245/3/032045>
- Jasiński, R. (2017b). *Research and modeling of masonry shear walls* (PhD, DSc thesis). Gliwice: Wydawnictwo Politechniki Śląskiej (in Polish). <https://doi.org/10.20944/preprints201806.0184.v1>
- Jasiński, R., Drobiec, Ł., & Mazur, W. (2019). Validation of selected non-destructive methods for determining the compressive strength of Masonry Units made of autoclaved aerated concrete. *Materials*, 12(3), 389. <https://doi.org/10.3390/ma12030389>
- Kubica, J. (2003). Niezbrojone ściany murowe poddane odkształceniom postaciowym wywołanym nierównomiernymi pionowymi przemieszczeniami podłoża. *Zeszyty Naukowe Politechniki Śląskiej. Budownictwo*, z. 96. Gliwice: Wydawnictwo Politechniki Śląskiej (in Polish).
- Majewski, S. (2003). *Mechanika betonu konstrukcyjnego w ujęciu sprężysto-plastycznym*. Gliwice: Wydawnictwo Politechniki Śląskiej (in Polish).
- Małyszko, L., Jemioło, S., Bilko, P., & Gajewski, M. (2015). *MES i modelowanie konstytutywne w analizie zniszczenia konstrukcji murowych. Tom 2 – Implementacja i przykłady*. Olsztyn: Wydawnictwo Uniwersytetu Warmińsko-Mazurskiego (in Polish).
- Menétrey, P., & Willam, K. J. (1995). Triaxial failure criterion for concrete and its generalization. *ACI Structural Journal*, 92(3), 311–318. <https://doi.org/10.14359/1132>
- Szojda, L. (2009). *Analiza numeryczna wpływu nieciągłych deformacji podłoża na budynki ścianowe*. Gliwice: Wydawnictwo Politechniki Śląskiej (in Polish).
- Wawrzynek, A., & Cińcio, A. (2005). *Adaptation of a plastic-damage concrete model for masonry material subjected to cyclic load*. Paper presented at Proceedings of the VIII International Conference on Computational Plasticity, COMPLAS VIII, Barcelona, Spain.
- Weihe, S. (1989). *Implicit integration schemes for multi-surface yield criteria subjected to hardening/softening behavior* (MS thesis). University of Colorado-Bulder.